Progress In Electromagnetics Research, Vol. 109, 211–227, 2010

BEAM-ABSENT ANALYSIS OF DISC-LOADED-COAXIAL WAVEGUIDE FOR APPLICATION IN GYRO-TWT (PART-1)

V. Kesari

Microwave Tube Research and Development Centre
Bangalore-13, India

Abstract—The electromagnetic field analysis of the disc-loaded-coaxial waveguide in two configurations was developed in TE-mode for its potential application in the fast-wave regime using the field matching technique at the cylindrical interface between disc-free and disc-occupied structure regions. The space harmonics were considered for the axial periodicity and the azimuthal harmonics were ignored for azimuthal symmetry of the present configurations. The dispersion and azimuthal interaction impedance characteristics obtained by present analysis were validated against those obtained by simulation software — HFSS within 0.1% and 0.5%, respectively. In special cases, the disc-loaded-coaxial structure reverts to well known conventional structures. The effect of structure parameters on the shape of dispersion characteristics was investigated in order to obtain a wideband-coalescence between the beam- and waveguide-mode dispersion characteristics, required for the wideband device performance, without deteriorating the azimuthal interaction impedance value.

1. INTRODUCTION

Extensive applications in the high power mm-wave regime, such as in high information density communications, long-range and high-resolution radars, space-debris and phased-array mapping radars, ground probing radars, electronic warfares, missile tracking and guidance, remote sensing, directed energy weaponries using high-power microwave, industrial heating, material processing, waste

Received 13 July 2010, Accepted 19 September 2010, Scheduled 22 October 2010
Corresponding author: V. Kesari (vishal_kesari@rediffmail.com).

remediation, plasma heating for controlled thermonuclear energy research, atmospheric purification of freons, ozone generation, advanced electron accelerators in high energy physics research, satellite power stations, and so on, attract the attention towards the gyro-devices like gyrotron, gyro-peniotron, gyro-backward-wave oscillator (gyro-BWO), gyroton, gyro-klystron, gyro-travelling-wave tube (gyro-TWT), slow-wave cyclotron amplifier (SWCA), cyclotron auto-resonance maser (CARM), auto-resonant peniotron, etc. [1–4]. Among the gyro-devices, the maximum consideration has been received by the gyrotron, the gyro-klystron and the gyro-TWT for their developments, however, for the applications, such as, phased-array radar, in which coherent power combining is required, an amplifier would be preferred to an oscillator. In addition, the data processing in radars becomes simpler and better while using an amplifier. Out of two gyro-amplifiers, the gyro-klystron and the gyro-TWT, which have been successfully developed so far, the first one that employs resonant interaction cavities has a lesser bandwidth than the second that uses a non-resonant waveguide interaction structure. That's why, the gyro-klystron amplifiers, which have potential application in linear accelerators, are not preferred to the gyro-TWTs, a wider bandwidth potential candidate, for its application in high information density communication systems and high-resolution radars in the high power, mm-wave regime [1–4].

Various structures were analyzed for its characteristics using various theoretical, numerical, experimental and simulation techniques for variety of electromagnetic applications [5–39]. A gyro-TWT usually uses a smooth-wall waveguide as an interaction structure that does not support single mode operation, needed for high-efficient device (competing action of neighboring modes) and exhibits a narrow bandwidth due to narrow band coalescence between the beam- and waveguide-mode dispersion characteristics. In the past, various interaction structures have been proposed for the gyro-TWT, for example, rectangular or circular waveguides in tapered or non-tapered cross-sections, in single-, two- or multi-stages, in tapered or non-tapered magnetic fields, with or without axial or azimuthal corrugations on the wall, with or without dielectric loading at the axis or on the wall, with or without lossy/ attenuator sections, etc. [2–4, 17–33]. It is obvious that, in order to achieve wideband performance of a gyro-TWT, one has to realize the grazing intersection between the beam- and waveguide-mode $\omega - \beta$ dispersion characteristics over a wide frequency range. One of the methods of broadbanding a gyro-TWT is to taper the cross-section of the waveguide and synchronously profile the magnetic field. This method gives wide bandwidth but at the cost

of device gain [17–19], because the different smaller length portions of the interaction length of different cross sections become effective for different frequency ranges over the amplification band of the device.

Denisov et al. [20–22] proposed a helical or spiral waveguide as an interaction structure for the enhancement of efficiency and bandwidth of the gyro-TWTs. The interaction structure introduced by Lawson et al. [4] contains elements of both linear and cyclotron resonance maser microwave tubes. They used an ideal sheath helix slow-wave structure to bunch a linearly streaming annular electron beam and a tapered circular waveguide was used to extract the microwave energy from beam via the gyrotron interaction. Agrawal et al. [19] also used the tapered circular waveguide, with tapered background magnetic field for broadband device performance but at the cost of device gain. Further, they have improved the device gain at the little decrease in bandwidth by projecting radial vane from the inner wall of waveguide interaction structure [19].

Although, the dielectric loading of smooth-wall circular waveguide, which has also been suggested, in literature [23–27], for wideband gyro-TWTs, promises for a wideband device performance but significantly reduces the power handling capability at a desired high-frequency of operation due to dielectric charging and associated dielectric heating in case of lossy dielectric. Thus, Choe and Uhm [28] and Leao et al. [29] suggested an all-metal structure, such as disc-loaded circular waveguide, for a wideband gyro-TWT performance, however, Choe and Uhm [28] have considered infinitesimally thin discs and lowest order space and modal harmonics in disc-free and disc-occupied regions, respectively. Kesari et al. [30] improved the theory of Choe and Uhm [28] by considering higher order space and modal harmonics. Further, they improved their own theory by considering the effect of finite disc thickness [31]. Furthermore, they tapered the disc-hole radius and the waveguide cross-section to result the wider gain-frequency response [18]. On the other hand, the coaxial waveguides were employed to exhibit high power level with reduced problem of mode competition [3, 33–36], if operation of device was required at higher order transverse electric modes instead of lower one. Kartikeyan et al. [37], following the method of Rao et al. [25, 26], proposed a coaxial waveguide interaction structure with dielectric lining on outer conductor for high power operation of a gyro-TWT. Also, a coaxial waveguide with axial vanes radially projecting inward from the wall of the waveguide was proposed by Qiu et al. [33] for its favor ability to suppress the mode competition by rarefying the eigenvalues and to strengthen the beam-wave interaction.

The present paper is developed around a disc-loaded-coaxial

waveguide in two configurations (Fig. 1). The configurations are field analyzed taking into account the space harmonics of propagating waves in disc-free region and the modal harmonics of stationary waves in the disc-occupied region between two consecutive discs (Section 2). A dispersion relation is obtained from the continuity of the field components at the interface between the two regions. The condition for non-trivial solution of the system of homogeneous equations, formed in the Fourier components of the field constants, gives the dispersion relation of the structure (Section 3).

The azimuthal interaction impedance is calculated for the structure assuming no power flow through the disc-occupied region (Section 4). Further, the effect of structure parameters is studied to control the shape of dispersion characteristics of the disc-loaded-coaxial waveguide for wideband coalescence between beam- and waveguide-mode dispersion characteristics for wide device bandwidth (Section 5). Finally, the conclusions drawn from the major findings are presented, pointing out the limitations of the work as well as the scope for the furtherance of the work.

2. STRUCTURE CONFIGURATIONS

In the present paper, two configurations of disc-loaded-coaxial waveguide, labeled as A and B, are considered (Fig. 1). In Configuration-A, metal discs are radially projecting inward from the metallic envelope, whereas in Configuration-B, metal discs are radially projecting outward from the coaxial insert (Fig. 1). In the past, a structure similar to Conf.-A was analyzed using field matching

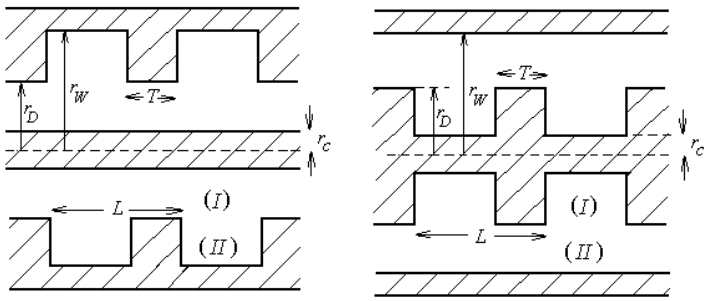

Figure 1. Longitudinal-view of disc-loaded-coaxial waveguide in two configurations developed on making a cut by a plane passing through its axis.

technique, however, for TM and HEM modes for the application of the structure in magnetically insulated transmission line oscillators (MILO) [38]. For the purpose of analysis, each configuration is divided into two analytical regions. In circular cylindrical system of coordinate $(r,\ \theta,\ z)$, radial extension $0 \le r \le r_C$ defines central metallic coaxial insert. The radial extension $r_C < r < r_D$ defines the disc-free region for Conf.-A and the disc-occupied region for Conf.-B, labeled as region I and the consecutive radial extension $r_D \le r \le r_W$ defines the disc-occupied region for Conf.-A and the disc-free region for Conf.-B, labeled as region II for the analysis, where r_C is the radius of coaxial insert, r_D the radius of disc-hole (Conf.-A) and the outer radius of disc (Conf.-B) and r_W the radius of waveguide (Fig. 1). The axial extensions $0 < z < (L-T)$ and $(L-T) \le z \le L$ of the disc-occupied region are the free-space region between two consecutive discs and metal disc region, respectively, where L and T are the periodicity of the structure and the disc-thickness, respectively.

The respective vanishing and increasing growth rate of TM ($H_Z = 0$) and TE ($E_Z = 0$) modes with frequency at or near the waveguide cutoff, where gyro-TWT is operated, the configurations are field analyzed in fast-wave regime for the TE mode excitation [17–39]. Considering stationary and traveling waves in disc-occupied and disc-free regimes of the axial periodic and azimuthal symmetric ($\partial/\partial\theta = 0$) structure, the field expressions for axial magnetic and azimuthal electric field intensities in regions I and II are given as [18, 30–32]:

$$H_z^p = \sum_{n=-\infty}^{+\infty} H_{z,\,n}^p = \sum_{n=-\infty}^{+\infty} A_n^p Z_0\{\gamma_n^p r\} \exp j\,(\omega\, t - \beta_n^p z) \tag{1}$$

$$H_z^q = \sum_{m=1}^{\infty} H_{z,\,m}^q = \sum_{m=1}^{\infty} A_m^q Z_0\{\gamma_m^q r\} \exp(j\omega\, t) \sin\,(\beta_m^q z) \tag{2}$$

and

$$E_\theta^p = \sum_{n=-\infty}^{+\infty} E_{\theta,\,n}^p = j\omega\,\mu_0 \sum_{n=-\infty}^{+\infty} \frac{1}{\gamma_n^p} A_n^p Z_0'\{\gamma_n^p r\} \exp j(\omega\, t - \beta_n^p z) \tag{3}$$

$$E_\theta^q = \sum_{m=1}^{\infty} E_{\theta,\,m}^q = j\omega\mu_0 \sum_{m=1}^{\infty} \frac{1}{\gamma_m^q} A_m^q Z_0'\{\gamma_m^q r\} \exp(j\omega\, t) \sin(\beta_m^q z), \tag{4}$$

where

$$Z_0\{\gamma_n^p r\} = \left\{ \begin{array}{l} [Y_0'\{\gamma_n^p r_C\} J_0\{\gamma_n^p r\} - J_0'\{\gamma_n^p r_C\} Y_0\{\gamma_n^p r\}] / Y_0'\{\gamma_n^p r_C\} \\ \qquad\qquad \text{Conf.-A} \\ [Y_0'\{\gamma_n^p r_W\} J_0\{\gamma_n^p r\} - J_0'\{\gamma_n^p r_W\} Y_0\{\gamma_n^p r\}] / Y_0'\{\gamma_n^p r_W\} \\ \qquad\qquad \text{Conf.-B} \end{array} \right\}$$

$$Z_0\{\gamma_m^q r\} = \left\{ \begin{array}{l} [Y_0'\{\gamma_m^q r_W\} J_0\{\gamma_m^q r\} - J_0'\{\gamma_m^q r_W\} Y_0\{\gamma_m^q r\}] / Y_0'\{\gamma_m^q r_W\} \\ \qquad\qquad \text{Conf.-A} \\ [Y_0'\{\gamma_m^q r_C\} J_0\{\gamma_m^q r\} - J_0'\{\gamma_m^q r_C\} Y_0\{\gamma_m^q r\}] / Y_0'\{\gamma_m^q r_C\} \\ \qquad\qquad \text{Conf.-B} \end{array} \right\}. \tag{5}$$

The superscripts $(p,\ q)$ refer to structure regions. $p = I$ with $q = II$ and $p = II$ with $q = I$ refer to configurations A and B, respectively. J_0 and Y_0 are the zeroth order Bessel functions of first and second kinds, respectively. The prime with a function indicates its derivative with respect to the argument. Referring to two regions, $\gamma_n^p = (k^2 - \beta_n^{p2})^{1/2}$ and $\gamma_m^q = (k^2 - \beta_m^{q2})^{1/2}$ are the radial or transverse propagation constants; β_n^p and β_m^q are the axial phase propagation constants; here k $(= \omega/c)$, being the free-space propagation constant and ω the angular frequency of the traveling wave. Following Floquet's theorem $\beta_n^p = \beta_0^p + 2\pi\, n/L$ in disc-free region, where n $(= 0,\ \pm 1,\ \pm 2,\ \pm 3,\ \ldots)$ is the traveling wave space harmonic number, and $\beta_m^q = m\pi/(L-T)$ in disc-occupied region, where m $(= 1,\ 2,\ 3,\ \ldots)$ is the stationary waves modal number.

3. DISPERSION RELATION

The relevant boundary conditions referring to the continuity of the axial magnetic and the azimuthal electric field intensities at the circular cylindrical interface $r = r_D$ can be mathematically expressed as

$$H_z^p = H_z^q \qquad \text{at } r = r_D, \quad 0 \le z < (L - T) \tag{6}$$

$$E_\theta^p = \left\{ \begin{array}{ll} E_\theta^q & \text{at } \ r = r_D, \ 0 \le z < (L-T) \\ 0 & \text{at } \ r = r_D, \ \ (L-T) \le z < L \end{array} \right. . \tag{7}$$

Substituting the field expressions from (1) and (2) into the boundary conditions (6) then multiplying both sides of the resulting relation by $\sin(\beta_m^q z)$, integrating with respect to z within the limit from $z = 0$ to $z = L - T$, and using orthogonal properties of trigonometric functions, one can get the series expression for A_m^q in terms of A_n^p. Similarly, starting from field expressions (3) and (4) and the boundary conditions (7) within integration limit $z = 0$ to $z = L$, one can get another series expression for A_m^q in terms of A_n^p. Further, two series expressions for A_m^q, thus obtained, can be equated to obtain a single

series equation involving A_n^p, that will be valid only for a particular m value. Thus, by varying m (= 1, 2, 3, ..., ∞), one can obtain infinite number of simultaneous series equations in terms of A_n^p. The vanishing determinant of the coefficients of A_n^p's, involved in infinite set of simultaneous homogeneous linear equations, will lead to the following dispersion relation of the analytical structure:

$$\det |\alpha_{n,m}| = 0; \tag{8}$$

where

$$\begin{aligned}
&\alpha_{n,m} \\
&= \frac{\beta_m^q}{(\beta_m^q)^2-(\beta_n^p)^2}\Big[LZ_0\{\gamma_n^p r_D\}Z_0'\{\gamma_m^q r_D\}(1-(-1)^m\exp[-j\beta_n^p(L-T)]) \\
&\quad /(L-T)-(\gamma_m^q/\gamma_n^p)Z_0'\{\gamma_n^p r_D\}Z_0\{\gamma_m^q r_D\} \\
&\quad [1-\exp(-j\beta_0^p L)\,(\cos(\beta_m^q L)+j\beta_n^p\sin(\beta_m^q L)/\beta_m^q)]\Big].
\end{aligned} \tag{9}$$

Conf.-A: $p = I$ and $q = II$; Conf.-B: $p = II$ and $q = I$.

4. AZIMUTHAL INTERACTION IMPEDANCE

For the fundamental space harmonic component of the traveling wave, the azimuthal interaction impedance, which is a measure of available azimuthal electric field at the vicinity of locus of centers of gyrating electrons in a gyro-TWT, may be defined as [32, 39]

$$K_{\theta,0}\{r\} = \left|E_{\theta,0}^p\{r\}\right|^2 /2\,(\beta_0^p)^2 P_t, \tag{10}$$

where P_t is the power transmitted through the structure, comprised of all the space harmonic components, which can be obtained by integrating half the real part of complex Poynting vector over the cross-sectional area of the disc-free region (region I: $r_C \le r \le r_D$ in Conf.-A and region II: $r_D \le r \le r_W$ in Conf.-B). It is being assumed that the propagation of RF waves does not take place inside the disc-occupied region (region II in Conf.-A and region I in Conf.-B) that presumably supports stationary waves (Fig. 1). Therefore, total power flow through the structure is given by:

$$P_t = \left\{ \begin{array}{ll} \pi \sum\limits_{n=-\infty}^{+\infty} \int\limits_{r=r_C}^{r=r_D} \left(E_{r,n}^I H_{\theta,n}^{I^*} - E_{\theta,n}^I H_{r,n}^{I^*}\right) rdr & \text{Conf.-A} \\ \pi \sum\limits_{n=-\infty}^{+\infty} \int\limits_{r=r_D}^{r=r_W} \left(E_{r,n}^{II} H_{\theta,n}^{II^*} - E_{\theta,n}^{II} H_{r,n}^{II^*}\right) rdr & \text{Conf.-B}\ . \end{array} \right\} \tag{11}$$

Substituting the field intensity components, $E^I_{\theta,n}$ from (2), each of E^p_r and H^p_θ equal to zero, satisfying the structure excitation in azimuthally symmetric TE modes, and $H^p_{r,\,n} = -j\beta^p_n A^p_n Z'_0\{\gamma^p_n r\} \exp j(\omega\, t - \beta^p_n z)/\gamma^p_n$, that is obtained by using the Maxwell's equation with (1); where the superscript p $(= I,\ II)$ refers disc-free region, into (11) one obtains:

$$P_t = \begin{cases} -\pi\,\omega\,\mu_0 \sum\limits_{n=-\infty}^{+\infty} \frac{\beta^p_n}{(\gamma^p_n)^2} (A^p_n)^2 \int\limits_{r=r_C}^{r=r_D} Z'^2_0\{\gamma^I_n r\} r dr & \text{Conf.-A} \\ -\pi\,\omega\,\mu_0 \sum\limits_{n=-\infty}^{+\infty} \frac{\beta^p_n}{(\gamma^p_n)^2} (A^p_n)^2 \int\limits_{r=r_D}^{r=r_W} Z'^2_0\{\gamma^{II}_n r\}\, r dr & \text{Conf.-B}\,. \end{cases} \tag{12}$$

5. RESULTS AND DISCUSSION

The dispersion relation (8) through (9) may be used for plotting the $\omega - \beta$ dispersion characteristics of the disc-loaded-coaxial waveguide. With the help of numerical methods in MATLAB, in-house computer code is developed for finding the roots of (8) and by progressively increasing the order of determinant involved in (8), the dispersion relation involving $n = 0,\ \pm1,\ \pm2,\ \pm3$, and $m = 1,\ 2,\ 3,\ 4,\ 5,\ 6,\ 7$ are found to be sufficient for converging solution (not shown here) as previously done in [30–32]. The azimuthal interaction impedance $K_{\theta,0}$ versus frequency characteristics may be plotted using (10), in which $E^p_{\theta,0}\{r\}$, obtainable from (3); β^p_0, obtainable from (8); and P_t, obtainable from (12); are substituted. The resulted expression involves a series containing A^p_n/A^p_0. For the purpose of estimating A^p_n/A^p_0, one can first represent A^p_n's $(-\infty < n < +\infty)$ in terms of a single constant, say A^q_1, by substituting the field expressions into the boundary condition (7) from (3) and (4), in which the latter is interpreted only for the fundamental modal harmonic $(m = 1)$, multiply both sides of resulting relation by $\exp(j\beta^p_n z)$, and integrate within the limit $0 \le z \le L$ using the orthogonal properties of trigonometric functions. Now, one may interpret A^p_0 in terms of A^q_1 that will give the expression of A^p_n/A^p_0 (free from A^q_1) in terms of propagation constants and structure parameters.

The analysis is restricted to azimuthally symmetric TE modes (TE_{0s}, where $s \ge 1$), however for the sake of simplicity results have been calculated only for the typically chosen lowest order TE_{01} mode. In general, in the present analysis one can calculate $K_{\theta,0}$ at any radial location within disc-free region where the electric field would be maximum for the beam-wave interaction with gyrating electron beam in the standpoint application of the structure in a gyro-TWT. For the

purpose of optimizing the beam position in both the configurations, the azimuthal interaction impedance characteristics are plotted for various sets of structure parameters in TE_{01} mode taking beam radius as a parameter and it has been found that $K_{\theta,0}$ maximizes around middle of the disc-free region, i.e., $r = (r_C + r_D)/2$ in Conf.-A and $r = (r_W + r_D)/2$ in Conf.-B.

For the special case of $r_C = 0$ in Conf.-A, from (5) $Z_0\{\gamma_n^p r_D\} = J_0\{\gamma_n^I r_D\}$ and $Z_0'\{\gamma_n^p r_D\} = J_0'\{\gamma_n^I r_D\}$ that makes the element $\alpha_{n,m}$ of the determinant involved in the dispersion relation (8) same as given in [31], thus the dispersion relation (8) passes to that for thick disc-loaded circular waveguide [31] (without coaxial insert), which further for the special case of $T \to 0$ passes to that for infinitely thin disc-loaded circular waveguide [30]. For the special case of $r_D/r_W = 1$ in Conf.-A and $r_D/r_C = 1$ in Conf.-B, (8) becomes $Z_0'\{\gamma_n^p r_W\} = 0$, which is the dispersion relation of the conventional coaxial waveguide (without discs) and for the special case of $r_D/r_W = 1$ with $r_C = 0$ in Conf.-A and $r_D = r_C = 0$ in Conf.-B, the dispersion relation (8) results $J_0'\{\gamma_n^I r_W\} = 0$, which is the well known dispersion relation of the conventional circular waveguide (without discs and coaxial insert) excited in the TE_{01} mode.

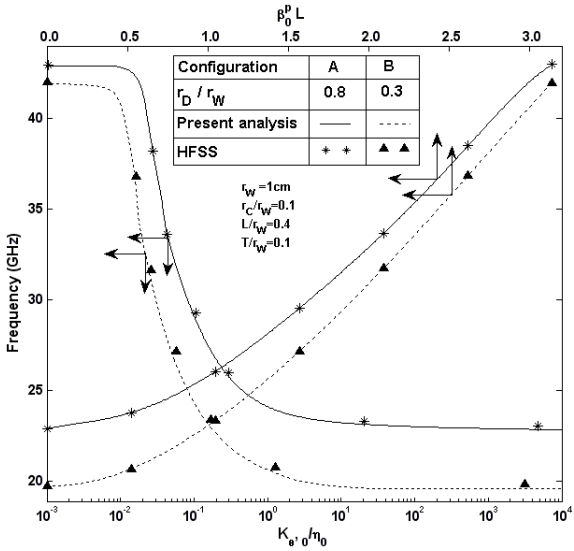

Figure 2. Dispersion and azimuthal interaction impedance characteristics of disc-loaded-coaxial waveguide in configurations A (solid curve) and B (broken curve), typically for TE_{01} mode excitation, obtained using present analysis validated against those obtained using HFSS.

The dispersion characteristics obtained by (8) and the azimuthal interaction impedance characteristics obtained by (10), closely agree with those obtained using HFSS — a commercially available simulation software — within 0.1% and 0.5% (Fig. 2), respectively, in both the configurations, for the typically chosen TE_{01} mode (Fig. 2). Similar to the disc-loaded waveguide [32], the azimuthal interaction impedance $K_{\theta,0}$ of both the configurations, for the typical structure parameters and typical coaxial waveguide mode TE_{01}, decreases with frequency from a very high positive value, at the lower cutoff frequency of the guide, via zero value, to a very high negative value, at the higher cutoff frequency of the guide (Fig. 2). One may correlate the azimuthal

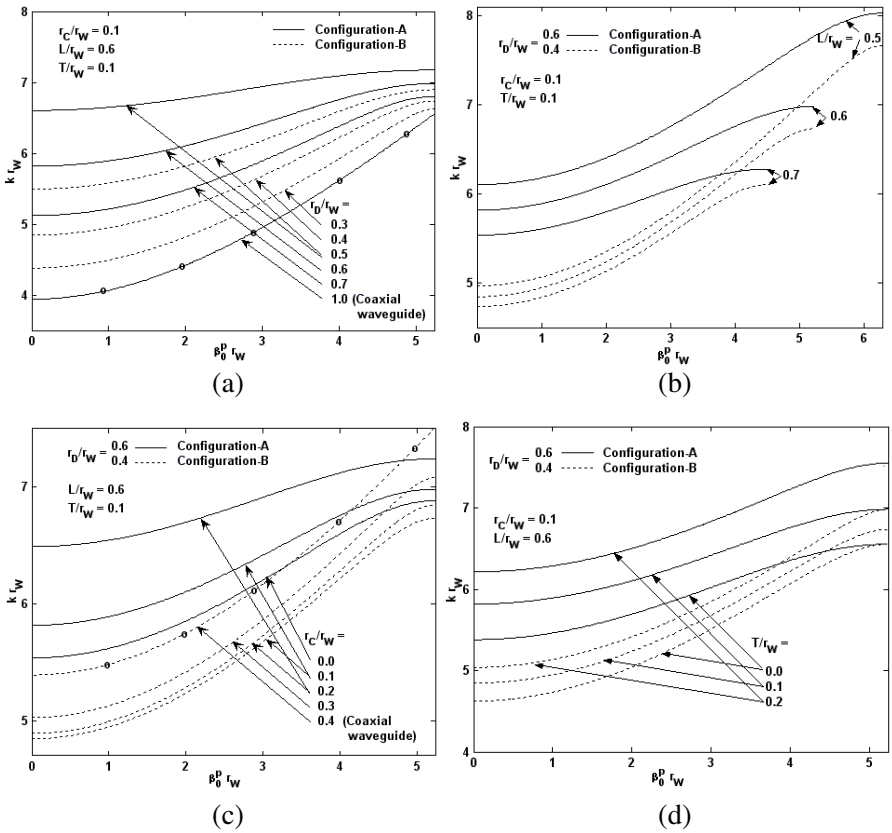

Figure 3. Dispersion characteristics of disc-loaded-coaxial waveguide in Conf.-A (solid curve) and Conf.-B (broken curve), typically for TE_{01} mode, taking (a) r_D/r_W, (b) L/r_W, (c) r_C/r_W and (d) T/r_W as the parameters.

interaction impedance characteristics of both the configurations with their dispersion characteristics, for which one has to interpret the power transmitted term P_t, appearing in the expression of $K_{\theta,0}$, equal to the group velocity of RF waves multiplied by the energy stored per unit length of the guide. In turn, it makes $K_{\theta,0}$ inversely proportional to the group velocity of RF waves. With an increase of frequency, the group velocities of RF waves (slope of the $\omega - \beta$ dispersion characteristics) at the lower and upper cutoff frequencies are each zero going positive and negative, respectively (Figs. 2 and 3). Thus, one may interpret the variation of azimuthal interaction impedance from high positive at lower cutoff frequency to high negative at upper cutoff frequency via zero value (Figs. 2 and 4) as aforementioned nature of variation of the group velocity.

The structure parameters, in general, enjoy the control over the passband and the shape of the dispersion characteristics (Fig. 3) as well as over the azimuthal interaction impedance characteristics (Fig. 4). Each of the lower and upper cutoff frequencies of the passband increases with the decrease and the increase of r_D/r_W in configurations A and B, respectively, however, amount of increase in upper cutoff frequency is relatively less than that of lower edge, that shortens the passband, for the typically chosen TE_{01} mode (Fig. 3(a)). This tells the decrease in passband with the decrease in disc-free cross-sectional region. On the other hand, with the increase of periodicity L/r_W (Fig. 3(b)) and the radius of coaxial insert r_C/r_W (Fig. 3(c)) passband shortens, accompanying a shift to lower and higher frequency ranges, respectively, in both the configurations. It is noticed that the upper and lower cutoff frequencies play dominant role in shortening the passband with the change in parameters L/r_W (Fig. 3(b)) and r_C/r_W (Fig. 3(c)), respectively. Whereas, the upper and lower cutoff frequencies of the passband shift to higher frequency range with the increase of disc thickness T/r_W (Fig. 3(d)) by approximately equal amount thereby the passband negligibly changes. The shift in passband is found to be more in Conf.-A than that of Conf.-B. Thus, the lower and upper cutoff frequencies decrease with the increase of disc-hole radius in Conf.-A and periodicity of both the configurations, whereas increase with the increase of disc radius in Conf.-B, radius of coaxial insert and disc thickness of both the configurations, such that the upper edge cutoff frequency is most sensitive to periodicity in both the configurations, whereas the lower cutoff frequency is most sensitive to radius of coaxial insert in Conf.-A and disc radius in Conf.-B, and the passband is most sensitive to periodicity.

For lower limiting value of r_D/r_W $(= r_C/r_W)$ dispersion characteristics, in Conf.-A, passes on to that of conventional coaxial

waveguide (without discs) (Fig. 3(a)) and in Conf.-B becomes a straight line parallel to β-axis (not shown) that gives zero group velocity of the wave in the circuit, that corresponds to the resonant frequency of closed circular cavities formed between two consecutive discs. Clearly, a control of the parameter r_D/r_W over the shape of dispersion characteristics can be visualized to obtain an optimized value of r_D/r_W for the wideband straight line portion of dispersion characteristics with references to wideband gyro-TWT performance. The flatter dispersion characteristics can be obtained with increasing either of L/r_W (Fig. 3(b)) or r_C/r_W (Fig. 3(c)), in Conf.-A, however, both of the parameters are insensitive to dispersion shaping close to waveguide

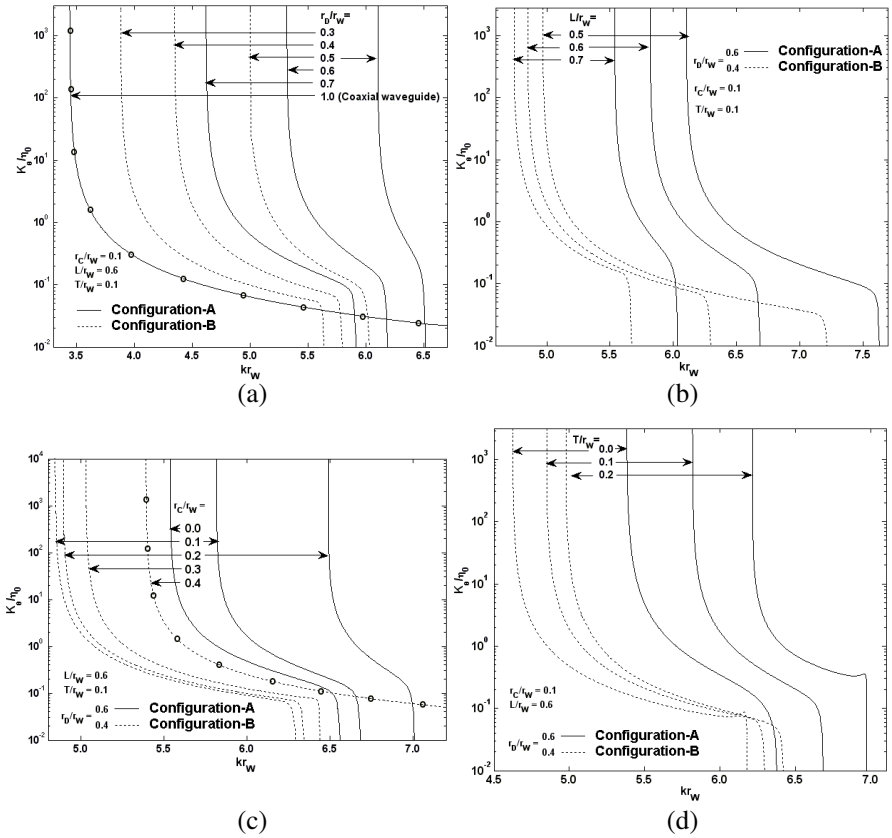

Figure 4. Azimuthal interaction impedance characteristics of disc-loaded-coaxial waveguide in Conf.-A (solid curve) and Conf.-B (broken curve), typically for TE_{01} mode excitation, taking (a) r_D/r_W, (b) L/r_W, (c) r_C/r_W and (d) T/r_W as the parameter.

cutoff in Conf.-B (Figs. 3(b) and 3(c)). Also, similar to earlier reported results [31] for the disc-loaded circular waveguide (without coaxial insert) the disc thickness T/r_W, in the presence of coaxial insert, is not effective in dispersion shaping (Fig. 3(d)). Although, similar to disc-loaded circular waveguide reported earlier [31], the disc periodicity is the most effective parameter for dispersion shaping in the presence of coaxial insert (Conf.-A), however coaxial insert radius is found to be an additional parameter for dispersion control.

The azimuthal interaction impedance $K_{\theta,\,0}$ versus frequency characteristics of both the configurations, for the special cases of $r_D = r_W$ with $r_C = 0$ in Conf.-A and $r_D = r_C = 0$ in Conf.-B, pass on to those for a smooth-wall waveguide given, for instance, in [17, 39]. Similar to a smooth-wall waveguide [17, 32, 39], for the special case of $r_D/r_W = 1$, $K_{\theta,\,0}$ decreases with frequency approaching zero value at very high frequencies in Conf.-A (coaxial waveguide), whereas becomes a straight line parallel to $K_{\theta,\,0}$-axis (not shown) in Conf.-B (Fig. 4(a)). The value of $K_{\theta,\,0}$ decreases with the increase and the decrease of r_D/r_W in configurations A and B, respectively. Thus, irrespective of the configurations, the value of $K_{\theta,\,0}$ increases with the introduction of discs in the guide except at higher frequencies, where it decreases rapidly to a value that is lower than that for a disc-free coaxial waveguide (Fig. 4(a)). The value of $K_{\theta,\,0}$ decreases with the increase of L/r_W (Fig. 4(b)), and with the decrease of r_C/r_W (Fig. 4(c)) and T/r_W (Fig. 4(d)) in both the configurations.

6. CONCLUSION

Out of the four parameters, namely r_D/r_W, L/r_W, r_C/r_W and T/r_W, with reference to two coaxial structures considered, the three parameters r_D/r_W, L/r_W and r_C/r_W in Conf.-A and only one parameter r_D/r_W in Conf.-B are sensitive to wideband dispersion shaping. Similar to disc-loaded circular waveguide (without coaxial insert) the periodicity and the disc thickness are the most and least responsible for the dispersion control, in the presence of coaxial insert (Conf.-A). In the presence of coaxial insert one can get an additional parameter to control the shape of dispersion characteristics. In Conf.-B, disc radius is the most sensitive to dispersion shaping, however, here also, disc thickness is the least sensitive to dispersion shaping. Thus, out of the two coaxial structures considered Conf.-A would be a comparatively better interaction structure for a wideband gyro-TWT with due consideration to azimuthal interaction impedance value. Further, one can optimize the structure parameters of a disc-loaded-coaxial waveguide to design the fast-wave device like gyro-TWT, for

desired wideband coalescence between beam-mode and waveguide-mode dispersion characteristic. This suggests the application of coaxial structures, previously predicted for high power oscillator devices, for wideband device performance in the presence of discs. Although, the structure is expected to its suitability for reduced problem of mode competition and high-efficient gyro-TWT, but the related study is kept out of the scope of the present paper for futuristic study.

REFERENCES

1. Granatstein, V. L. and I. Allexeff, *High-power Microwave Sources*, Artech House, Norwood, Massachusetts, 1987.
2. Chu, K. R., "The electron cyclotron maser," *Rev. Mod. Phys.*, Vol. 76, No. 2, 489–540, May 2004.
3. Thumm, M., "State-of-the-art of high-power gyro-devices and free electron masers," Scientific Report FZKA 6224, Forschungszentrum Karlsruhe, Germany, Jan. 2008.
4. Lawson, W., A. Fernandez, T. Hutchings, and G. P. Saraph, "A novel hybrid slow-wave/fast-wave traveling-wave amplifier," *IEEE Trans. Plasma Sci.*, Vol. 25, No. 5, 1150–1154, Oct. 1997.
5. Kumar, D., P. K. Choudhury, and O. N. Singh, "Towards the dispersion relations for dielectric optical fibers with helical windings under slow- and fast-wave considerations — A comparative analysis," *Progress In Electromagnetics Research*, Vol. 80, 409–420, 2008.
6. Reutskiy, S. Y., "The methods of external excitation for analysis of arbitrarily-shaped hollow conducting waveguides," *Progress In Electromagnetics Research*, Vol. 82, 203–226, 2008.
7. Su, D. Y., D.-M. Fu, and Z.-H. Chen, "Numerical modeling of active devices characterized by measured S-parameters in FDTD," *Progress In Electromagnetics Research*, Vol. 80, 381–392, 2008.
8. Naqvi, A., A. Hussain, and Q. A. Naqvi, "Waves in fractional dual planar waveguides containing chiral nihility metamaterial," *Journal of Electromagnetic Waves and Applications*, Vol. 24, Nos. 11–12, 1575–1586, 2010.
9. Zhang, X. F., L. F. Shen, J.-J. Wu, and T.-J. Yang, "Backward guiding of terahertz radiation in periodic dielectric waveguides," *Journal of Electromagnetic Waves and Applications*, Vol. 24, No. 4, 557–564, 2010.
10. Xu, J., W. X. Wang, L. N. Yue, Y. B. Gong, and Y. Y. Wei, "Electromagnetic wave propagation in an elliptical chiroferrite

waveguide," *Journal of Electromagnetic Waves and Applications*, Vol. 23, Nos. 14–15, 2021–2030, 2009.

11. Topa, A. L., C. R. Paiva, and A. M. Barbosa, "Guidance and leakage behavior of uniaxial ridge waveguides," *Journal of Electromagnetic Waves and Applications*, Vol. 23, No. 13, 1675–1684, 2009.
12. Pérez, A. M., V. E. Boria, B. Gimeno, S. Anza, C. Vicente, and J. Gil, "Multipactor analysis in circular waveguides," *Journal of Electromagnetic Waves and Applications*, Vol. 23, Nos. 11–12, 1575–1583, 2009.
13. Siong, C. C. and P. K. Choudhury, "Propagation characteristics of tapered core helical cald dielectric optical fibers," *Journal of Electromagnetic Waves and Applications*, Vol. 23, Nos. 5–6, 663–674, 2009.
14. Zhu, Z. J. and B. F. Jia, "π-Mode stopband characteristics caused by asymmetries of support rod and loaded metal in helix structures," *Journal of Electromagnetic Waves and Applications*, Vol. 22, Nos. 14–15, 2077–2085, 2008.
15. Shen, L. F. and Z. H. Wang, "The propagation characteristics in a doubly clad optical fiber including left-handed materials," *Journal of Electromagnetic Waves and Applications*, Vol. 22, No. 7, 895–904, 2008.
16. Soekmadji, H., S. L. Liao, and R. J. Vernon, "Trapped mode phenomena in a weakly overmoded waveguiding structure of rectangular cross section," *Journal of Electromagnetic Waves and Applications*, Vol. 22, No. 1, 143–157, 2008.
17. Singh, G., S. M. S. Ravi Chandra, P. V. Bhaskar, P. K. Jain, and B. N. Basu, "Analysis of dispersion and interaction impedance characteristics of an azimuthally-periodic vane-loaded cylindrical waveguide for a gyro-TWT," *Int. J. Electronics*, Vol. 86, No. 12, 1463–1479, Dec. 1999.
18. Kesari, V., P. K. Jain, and B. N. Basu, "Exploration of a double-tapered disc-loaded circular waveguide for a wideband gyro-traveling-wave tube," *IEEE Electron Dev. Lett.*, Vol. 27, No. 3, 194–197, Mar. 2006.
19. Agrawal, M., G. Singh, P. K. Jain, and B. N. Basu, "Analysis of a tapered vane loaded broad-band gyro-TWT," *IEEE Trans. Plasma Sci.*, Vol. 29, No. 3, 439–444, Jun. 2001.
20. Denisov, G. G., V. L. Bratman, A. D. R. Phelps, and S. V. Samsonov, "Gyro-TWT with a helical operating waveguide: New possibilities to enhance efficiency and frequency bandwidth," *IEEE Trans. Plasma Sci.*, Vol. 26, No. 3, 508–518, Jun. 1998.

21. Cooke, S. J. and G. G. Denisov, "Linear theory of a wide-band gyro-TWT amplifier using spiral waveguide," *IEEE Trans. Plasma Sci.*, Vol. 26, No. 3, 519–530, Jun. 1998.
22. Denisov, G. G., V. L. Bratman, A. W. Cross, W. He, A. D. R. Phelps, K. Ronald, S. V. Samsonov, and C. G. Whyte, "Gyrotron traveling wave amplifier with a helical interaction waveguide," *Phys. Rev. Lett.*, Vol. 81, No. 25, 5680–5683, Dec. 1998.
23. Choe, J. Y. and H. S. Uhm, "Analysis of the wide band gyrotron amplifier in dielectric loaded waveguide," *J. Appl. Phys.*, Vol. 52, No. 7, 4508–4516, Jun. 1981.
24. Choe, J. Y., H. S. Uhm, and S. Ahn, "Slow wave gyrotron amplifier with a dielectric center rod," *IEEE Trans. Microwave Theory Tech.*, Vol. 30, No. 5, 700–707, May 1982.
25. Rao, S. J., P. K. Jain, and B. N. Basu, "Two-stage dielectric loading for broadbanding a gyro-TWT," *IEEE Electron. Dev. Lett.*, Vol. 17, No. 6, 303–305, Jun. 1996.
26. Rao, S. J., P. K. Jain, and B. N. Basu, "Broadbanding of a gyro-TWT by dielectric-loading through dispersion shaping," *IEEE Trans. Electron Dev.*, Vol. 43, No. 12, 2290–2299, Dec. 1996.
27. Rao, S. J., P. K. Jain, and B. N. Basu, "Hybrid-mode helix-loading effects on gyro-travelling-wave tubes," *Int. J. Electron.*, Vol. 82, No. 6, 663–675, Jun. 1997.
28. Choe, J. Y. and H. S. Uhm, "Theory of gyrotron amplifiers in disc or helix loaded waveguides," *Int. J. Electron.*, Vol. 53, No. 6, 729–741, Jun. 1982.
29. Leou, K. C., T. Pi, D. B. Mcdermott, and N. C. Luhmann, Jr., "Circuit design for a wideband disc loaded gyro-TWT amplifier," *IEEE Trans. Plasma Sc.*, Vol. 26, No. 3, 488–495, Jun. 1998.
30. Kesari, V., P. K. Jain, and B. N. Basu, "Analytical approaches to a disc loaded cylindrical waveguide for potential application in wideband gyro-TWTs," *IEEE Trans. Plasma Sci.*, Vol. 32, No. 5, 2144–2151, Oct. 2004.
31. Kesari, V., P. K. Jain, and B. N. Basu, "Analysis of a circular waveguide loaded with thick annular metal discs for wideband gyro-TWTs," *IEEE Trans. Plasma Sci.*, Vol. 33, No. 4, 1358–1365, Aug. 2005.
32. Kesari, V., P. K. Jain, and B. N. Basu, "Analysis of a disc-loaded circular waveguide for interaction impedance of a gyrotron amplifier," *Int. J. Infrared and Millimeter Waves*, Vol. 26, No. 8, 1093–1110, Aug. 2005.

33. Qiu, C. R., Z. B. Ouyang, S. C. Zhang, H. B. Zhang, and J. B. Jin, "Self-consistent nonlinear investigation of an outer-slotted-coaxial waveguide gyrotron traveling-wave amplifier," *IEEE Trans. Plasma Sci.*, Vol. 33, No. 3, 1013–1018, Jun. 2005.
34. Vlasov, S. N., L. I. Zagryadskaya, and I. M. Orlova, "Open coaxial resonators for gyrotrons," *Radio Eng. Electron. Physics*, Vol. 21, No. 5, 96–102, May 1976.
35. Iatrou, C. T., S. Kern, and A. B. Pavelyev, "Coaxial cavities with corrugated inner conductor for gyrotrons," *IEEE Trans. Microwave Theory Tech.*, Vol. 44, No. 1, 56–64, Jan. 1996.
36. Nusinovich, G. S., M. E. Read, O. Dumbrajs, and K. E. Kreischer, "Theory of gyrotrons with coaxial resonators," *IEEE Trans. Electron Dev.*, Vol. 41, No. 3, 433–438, Mar. 1994.
37. Kartikeyan, M. V., C. T. Iatrou, and M. Thumm, "A coaxial gyro-TWT," *IEEE Trans. Plasma Sci.*, Vol. 29, No. 1, 57–61, Feb. 2001.
38. Wang, D., Z. Fan, D. Chen, and J. Deng, "Rigorous analysis of the coaxial disk-loaded waveguide slow-wave structures," *Proc. Int. Conf. Microwave and Millimeter Wave Tech.*, 1–4, Apr. 18–21, 2007.
39. Sangster, A. J., "Small-signal analysis of the travelling-wave gyrotron using Pierce parameters," *Proc. IEE*, Vol. 127, No. 2, 45–52, Apr. 1980.